Plasmonics (2025) 20:6785–6794
https://doi.org/10.1007/s11468-025-03024-1

RESEARCH

Photonic Crystal Fiber Sensor Based on Surface Plasmon Resonance Sensor with Ultra-High Sensitivity

Fengrui Yang[1] · Jingwei Lv[1] · Wei Liu[1] · Jianxin Wang[1] · Xili Lu[2] · Lin Yang[1] · Qiang Liu[1] · Paul K. Chu[3] · Chao Liu[1]

Received: 24 March 2025 / Accepted: 9 May 2025 / Published online: 24 May 2025

Abstract

An ultra-sensitive photonic crystal optical fiber sensor based on surface plasmon resonance (SPR) is designed and analyzed. The D-shaped optical fiber is symmetrically coated with two layers of gold along the *Y*-axis, and the pores inside the fiber follow the PCF stacking structure. The D-symmetric double gold layer structure is based on the surface dissociative excitation resonance excitation mechanism, and the Y-symmetric double gold layer design enhances the electromagnetic coupling at the metal-medium interface, providing more stable excitation conditions for the SPR effect. This structure can effectively modulate the propagation characteristics of the surface plasma wave, thereby improving the response of the sensor to changes in refractive index. The sensing characteristics are investigated using the finite element method. It shows ultra-high sensitivity and low loss, as exemplified by a maximum wavelength sensitivity of 70,000 nm/*RIU*, an average wavelength sensitivity of 5150 nm/*RIU* in the *RI* range between 1.23 and 1.43. In addition, the sensor has a resolution of 1.43×10^{-7} *RIU*, a factor of merit (*FOM*) of 834.4 RIU^{-1}, and a maximum loss of only 2.59 dB/cm, greatly improving optical transmission efficiency. The outstanding results suggest immense in various applications, including biosensing, virus detection, and organic chemistry.

Keywords Surface plasmon resonance · Photonic crystals · Optical fibers · Sensing · Refractive index

Introduction

Surface plasmon resonance (SPR) is highly sensitive to the external refractive index (RI) and has been widely applied to biomedicine and environmental monitoring [1, 2]. However, the traditional prism-coupler-based SPR sensor is unwieldy and intricate, rendering it impractical for remote measurements [3, 4]. Accordingly, device miniaturization is highly important [5]. The photonic crystal fiber (PCF) is a two-dimensional photonic crystal [6] with the core consisting of solid silica or air holes and the cladding containing regularly distributed air holes [7]. Hence, it has a porous or microstructure [8]. The PCF offers a number of advantages, such as its small size, resistance to electromagnetic interference, and flexible cladding [9]. In fact, the PCF-based SPR sensor has been demonstrated to offer high-performance RI sensing and has attracted considerable research and commercial interest [10, 11], for instance, medical diagnostics [12, 13], biomolecular analysis [14, 15], antigen–antibody interactions [16], and security and environmental monitoring [17].

A variety of PCF structures have been proposed, including double D-shape structures [18, 19], H-shaped structures [20], and multi-channel sensing structures [21]. These structures can be broadly classified into two categories: internal sensing and external sensing. In internal sensing, the pores in the fibers are selectively filled with the analyte, whereas in external sensing, the analyte is deposited on the surface of the sensor. However, thin metal film deposition and analyte injection into specific holes can be challenging and time-consuming in comparison with the use of surface coatings. Therefore, it is more practical to adopt external sensing [22].

Parthiban et al. have proposed a PCF sensor with a composite film composed of Ag and MgF_2 [23], showing a maximum wavelength sensitivity of 20,000 nm/*RIU*, but

✉ Chao Liu
msm-liu@126.com

1 School of Physics and Electronic Engineering, Northeast Petroleum University, Daqing 163318, China

2 School of Materials Science and Chemical Engineering, Harbin Engineering University, Harbin 150001, China

3 Department of Physics, Department of Materials Science and Engineering, and, Department of Biomedical Engineering, City University of Hong Kong, Tat Chee Avenue, Kowloon, Hong Kong, China

the sensitivity is not satisfactory. Gold, as the plasmonic medium, produces a more pronounced resonance peak shift than other metals. Su et al. have designed a PCF sensor coated with a gold ring [24], showing a maximum wavelength sensitivity of 35,943 nm/*RIU*, but the gold adds to the cost. Mohammad et al. have proposed a PCF sensor coated with the Au-TiO_2 composite film [25] polished on both sides, showing a maximum wavelength sensitivity of 61,000 nm/*RIU*. However, it exhibits a maximum loss of 600 dB/cm and a low transmission efficiency. Herein, a symmetrical D-type PCF structure is designed. The gold film is symmetric along the *Y*-axis and partially deposited on the D-shaped surface to enhance the SPR. The choice of depositing the gold film in the partially polished area is based on the excitation conditions and the light field distribution characteristics of the surface equipartition exciton resonance. Partial deposition allows precise control of the electromagnetic field coupling strength at the metal–dielectric interface and avoids over-absorption or scattering of the optical field caused by full-area deposition. This design concentrates the SPR effect in the critical sensing region, which improves the modulation efficiency of the optical signal by the refractive index change. If a gold film were to be deposited over the entire polished area, excessive gold coverage would cause the optical field to be strongly absorbed by the gold layer, which would reduce sensitivity and increase losses. Moreover, the complexity would be greatly increased, increasing the difficulty and cost of the preparation process and potentially introducing more uncontrollable factors (e.g., uneven thickness of the gold film), which is detrimental to the stability and reproducibility of the sensor. Our analysis shows that this structure has excellent characteristics, including a maximum wavelength sensitivity of 70,000 nm/*RIU*, an average wavelength sensitivity of 5150 nm/*RIU*, a figure of merit (*FOM*) of 834.4 RIU^{-1}, and a maximum loss of only 2.59 dB/cm in the wavelength range between 0.49 and 1.52. The sensing characteristics are superior to those of similar *RI* sensors reported previously, rendering the sensor suitable for a wide range of applications, including biosensing, virus detection, and organic chemistry.

Structure and Analysis

Figure 1 (a) and (b), respectively, depict the two-dimensional and three-dimensional cross sections of the PCF-SPR sensor. The simulation process is carried out using COMSOL Multiphysics v6.1 software, and the numerical analysis is performed using the finite element method. In order to accurately simulate the light propagation and surface plasmon resonance effects of the photonic crystal fiber sensor, the computational domain covers the entire D-shaped fiber and the surrounding medium area. The outer computational

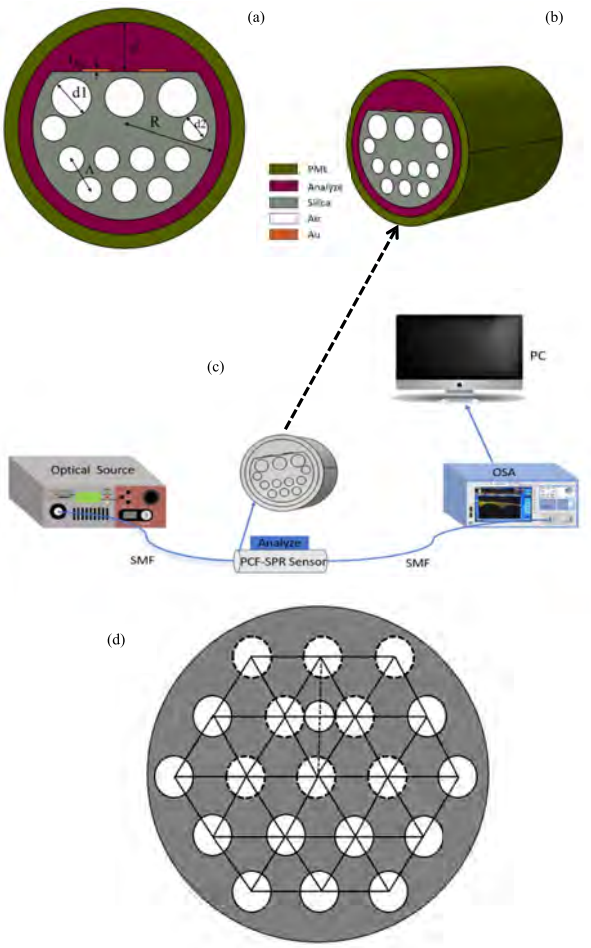

Fig. 1 (**a**) Cross-section of the PCF-SPR sensor; (**b**) three-dimensional view; (**c**) transmission; and (**d**) stacked structure

domain is extended by 10 μm in all directions to ensure that the boundary conditions do not affect the internal electromagnetic field distribution. A perfectly matched 1-μm thick layer is used in the boundary conditions to effectively absorb the outgoing light and prevent reflections from affecting the simulation results. A free tetrahedral mesh is used to subdivide the model, and to improve computational accuracy, local encryption is applied to the core region of the optical fiber, the gold film layer and the contact region of the medium to be measured. The model contains 22 domains, 92 boundaries, and 90 vertices. The simulation uses a frequency domain solver with approximately 72,000 total degrees of freedom, covering both electric and magnetic field components. The accuracy of the results is ensured by a residual convergence criterion during the solution process. In the analysis, the radius of the fiber is $r = 7.5$ μm, and the air holes are arranged in accordance with the structure of the PCF stack, as illustrated in Fig. 1 (d). The radius of the larger aperture, d_1, is 1.4 μm, while that of the smaller aperture, d_2,

is 0.9 μm. Two 28-nm-thick gold films are deposited by magnetron sputtering or chemical vapor deposition (CVD) on the surface with a *Y*-axis symmetry. The outer layer serves as the perfect match layer to absorb scattered light and prevent scattering. As shown in Fig. 1 (c), the analyte droplet is placed on the surface, and the single-mode optical fiber is connected on both ends. Light emitted from the source passes through the sensor and reaches the spectrometer, which outputs the data to a computer for analysis.

The finite element method is employed to determine the characteristics of the sensor. The main body of the sensor is composed of SiO_2. The RI variation with wavelength can be calculated using the Sellmeier dispersion relation [26]:

$$n^2{}_{Silica} - 1 = \frac{A_1\lambda^2}{\lambda^2 - B_1^2} + \frac{A_2\lambda^2}{\lambda^2 - B_2^2} + \frac{A_3\lambda^2}{\lambda^2 - B_3^2} \tag{1}$$

where $A1 = 0.6961663$, $A2 = 0.4079426$, $A3 = 0.8974794$, $B1 = 0.0684043$, $B2 = 0.1162424$, and $B3 = 9.896161$. The dielectric constant of gold is determined according to the Drude-Lorentz model [27]:

$$\varepsilon_{Au} = \varepsilon_\infty - \frac{\omega_D^2}{\omega(\omega + i\gamma_D)} - \frac{\triangle\varepsilon\ \Omega_L^2}{(\omega^2 - \Omega_L^2) + i\Gamma_L\omega} \tag{2}$$

where 5.9673 is the high-frequency permittivity of Au; 1.09 is the weighting factor; and $\omega_D/2\pi$ and $\gamma_D/2\pi$ are the plasma frequency and damping frequency with values of 2113.6 THz and 15.92 THz, respectively. $\Gamma_L/2\pi = 104.86$ THz and $\Omega/2\pi = 650.07$ THz are the spectral width and spectral frequency of the Lorentz oscillator, respectively.

Results and Discussion

The confinement loss (*CL*) spectrum is derived by the following equation [28]:

$$CL(dB/cm) = 8.686 \times \frac{2\pi}{\lambda} \times Im\left(n_{eff}\right) \times 10^4 \tag{3}$$

where "n_{eff}" represents the imaginary component of the effective *RI* of the fiber mode field. Figure 2 (a) presents the CL spectrum for an analyte *RI* of 1.42. The red solid line and red dashed line represent the real part of the effective *RI* of the y-polarized fundamental mode and the SPP mode, respectively. The two lines intersect at a wavelength of 825 nm. This indicates that the phase-matching condition for surface plasmon resonance is satisfied, resulting in the coupling of the y-polarized fundamental mode to the SPP mode.

As shown in Fig. 2 (b and c), at the resonant wavelength, the y-polarized fundamental mode is confined within the fiber core, and the energy distribution of the SPP mode is close to the gold film. The loss spectrum of the x-pol fundamental mode, indicated by the black dashed line in Fig. 2 (a), is smaller than that of the y-polarized fundamental mode, which depends strongly on the localization of the plasmonic medium. Therefore, the sensor must be able to receive incident light polarized in the *y* direction. In the subsequent optimization process, the loss spectrum of the y-polarized fundamental frequency mode is adopted.

The wavelength sensitivity (WS), which serves as an essential metric to gauge the efficacy of the sensor, is defined as the ratio of the discrepancy of the resonant wavelengths for different refractive indexes to the disparity in the refractive indexes themselves [29]:

$$S(\lambda, n) = \frac{\triangle\lambda}{\triangle n}(nm/RIU) \tag{4}$$

The wavelength resolution (*R*) reflects the sensitivity of the sensor to minor alterations in wavelength and the capability to discern subtle changes in the RI of the analyte. A lower resolution indicates a greater sensitivity to alterations in the RI as shown in the following [30]:

$$R = \frac{\triangle n_a \times \Delta\lambda_{min}}{\triangle\lambda_{peak}} = \frac{\triangle\lambda_{min}}{S_\lambda}(RIU) \tag{5}$$

Conversely, a narrower full-width at half-maximum (*FWHM*) of the loss spectrum corresponds to a higher resolution, which can be quantified by the quality factor, the figure of merit (*FOM*) defined as follows [31]:

$$FOM = \frac{S_\lambda}{FWHM}\left(RIU^{-1}\right) \tag{6}$$

The various structural parameters of the sensor are optimized beginning with the thickness of the gold film. When the incident light wave traverses the optical fiber and interacts with the metal film, free electrons in the film oscillate collectively in response to the electric field creating a surface plasmonic wave. According to the principle of surface plasmon resonance, when a light wave is transmitted along an optical fiber and interacts with a metal film layer, the free electrons in the metal film generate collective oscillations due to the excitation of the electromagnetic field of the light wave. These oscillations in turn excite the surface plasma wave. As the core medium of energy conversion, the thickness of the gold film directly affects the energy coupling efficiency between the photonic crystal fiber and thus greatly affects the sensing performance. Five gold film thicknesses ranging from 26 to 34 nm are analyzed. Figure 3 (a) shows notable shifts in the spectra with different film thicknesses, and Fig. 3 (b) compares the sensitivity, revealing the best sensitivity when the gold film thickness is 28 nm. Consequently, this value is adopted in the subsequent investigation.

The polishing depth is then optimized. The polishing depth determines the proximity of the fiber surface to the external material to be measured, and thus the strength of the interaction between the Swift field and the material to be measured. Figure 4 (a) shows the loss spectra for polishing

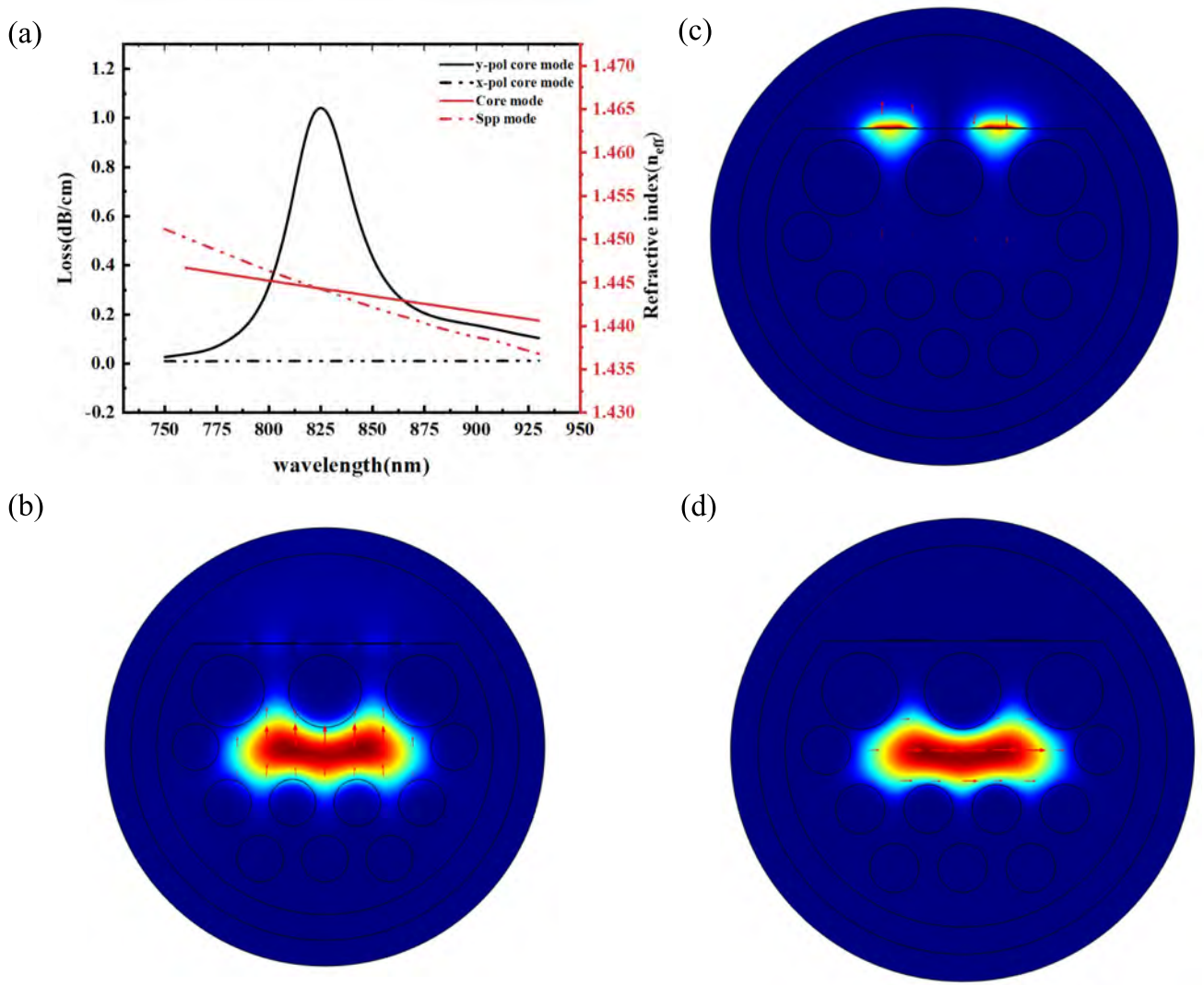

Fig. 2 **a** Limiting loss spectrum of the PCF-SPR sensor for an analyte RI of 1.42; **b** electric field distribution of the y-polarized mode; **c** electric field distribution of the SPP mode; and **d** electric field distribution of the x-polarization mode

depths of 3.1, 3.3, 3.5, and 3.7 µm, disclosing the significant impact of the polishing depth on the resonance wavelength and loss. Figure 4 (b) shows that the sensor delivers the best performance when the polishing depth is 3.5 µm, which is adopted in the subsequent study.

The effects of the size of the air holes are analyzed. According to the fiber theory, varying the aperture size changes the effective refractive index distribution within the fiber cross section. This in turn modulates the degree of optical field confinement and the transmission characteristics. Changes in the optical properties described above are directly related to sensor sensitivity, resonant wavelength, and other key performance metrics. The larger air holes are optimized first, and 1.2, 1.3, and 1.4 µm are chosen as the radii. Figure 5 (a) and (b) show the loss spectrum and wavelength sensitivity of the sensor versus aperture radius, respectively. The sensor shows the optimal sensitivity when the air hole radius is 1.4 µm, which is used in our subsequent analysis.

The dimensions of the small air apertures are optimized using 0.8, 0.9, and 1 µm in the analysis. Figure 6 (a) presents the loss spectra, while Fig. 6 (b) shows the sensitivity. The optimal characteristics are achieved when the radius is 0.9 µm, and this value is chosen.

By adopting the gold layer thickness (t_{Au}) of 28 nm, polishing depth (d) of 3.5 µm, large air hole radius (d_1) of 1.4 µm, and small air hole radius (d_2) of 0.9 µm, and wavelength range between 500 and 1600 nm, excellent transmission characteristics, high sensitivity, and optimal performance are accomplished. Our analysis reveals that the sensor delivers the most favorable performance between 800 and 1550 nm. In the coating process, magnetron sputtering technology

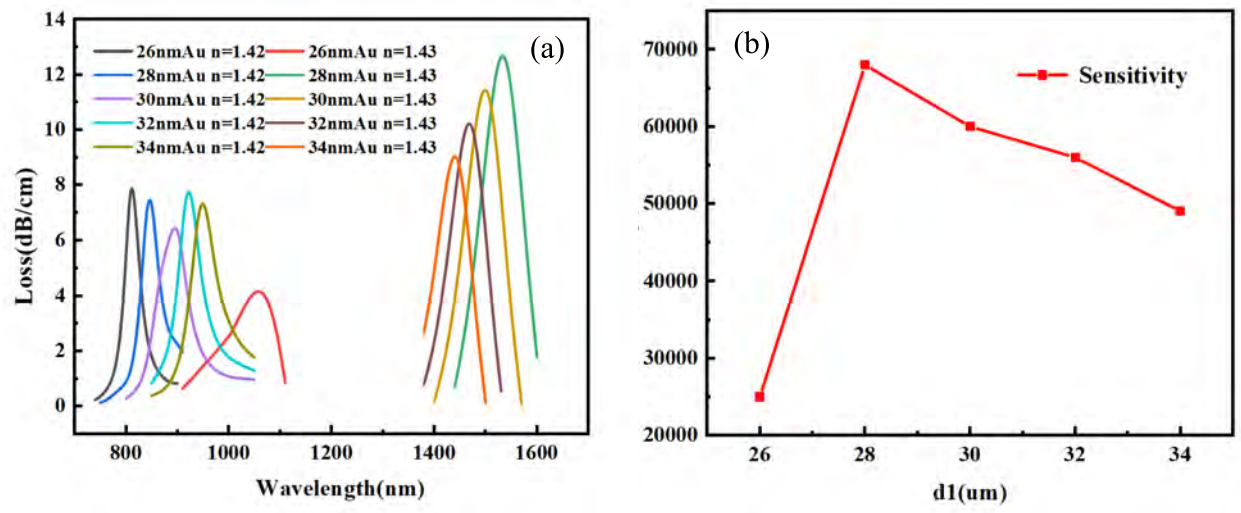

Fig. 3 **a** Loss spectra for different gold film thicknesses; **b** comparison of the sensitivity of gold films with different thicknesses

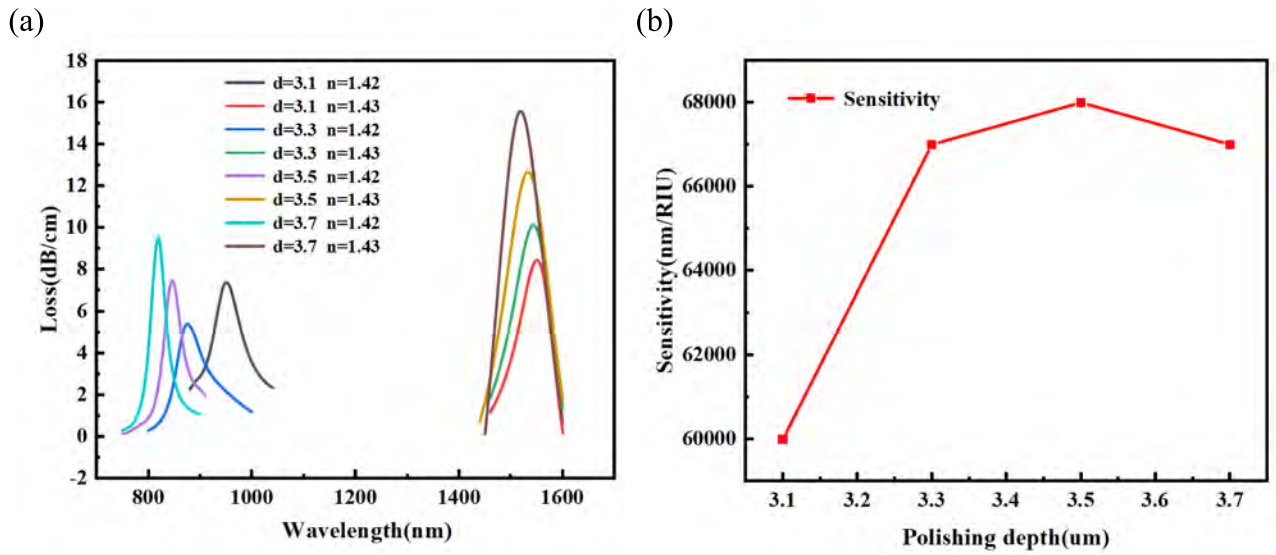

Fig. 4 **a** Loss spectra for different polishing depths; **b** comparison of the sensitivity for different polishing depths

can be used, which is a mature physical vapor deposition technology, through the use of magnetic field constraints on the movement of electrons in a high-vacuum environment, so as to make argon gas ionization and bombardment of the gold target, the gold atoms will be sputtered onto the substrate to form a thin film. During the magnetron sputtering process, we can precisely control the thickness and uniformity of the gold film by precisely controlling the parameters such as sputtering power, time, air pressure, and the distance between the target material and the substrate to realize the high-precision control of the thickness of the 28-nm gold film. And the high-precision chemical–mechanical polishing technology can be used in the polishing process. This technology flattens the surface of the sample by applying a certain pressure between the sample and the polishing pad, and using a polishing solution containing abrasive particles and chemical reagents, under the combined effect of grinding and chemical reaction. By precisely controlling factors such as polishing time, pressure, polishing solution composition, and flow rate, good control of the 3.5 μm polishing accuracy can be achieved. The photonic crystal fiber structure and thin film deposition process used in this study are based on mature technologies. Optical fiber drawing and polishing can be standardized by automated equipment, and magnetron

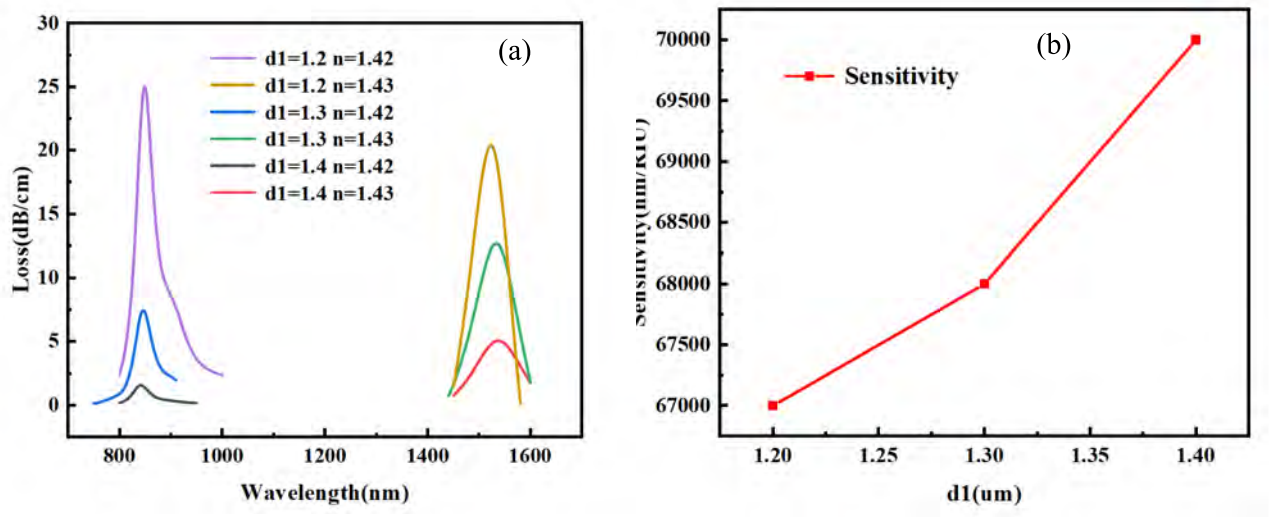

Fig. 5 **a** Loss spectra for different d_1; **b** comparison of the sensitivity for different d_1

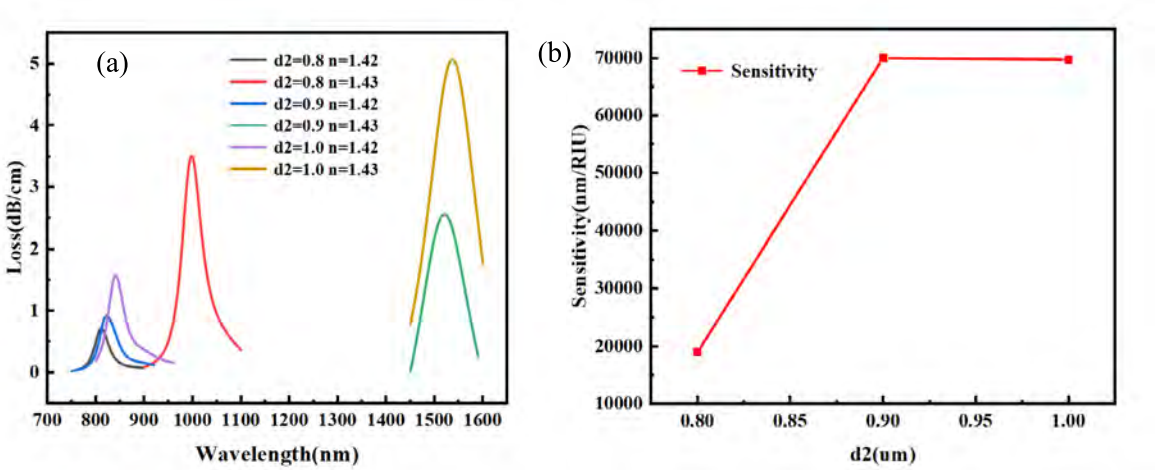

Fig. 6 **a** Loss spectra for different d_2; **b** comparison of the sensitivity for different d_2

sputter deposition technology has also been widely used in industrial production, which can meet the precision requirements of large-scale manufacturing. At the same time, the design simplifies the structure and reduces the special process, which reduces the manufacturing difficulty and cost.

Figure 7 (a) and (b) show the tendency to shift toward longer wavelengths with progressively larger peaks as the *RI* increases. As the refractive index of the external environment increases, the interaction between the Swift field at the fiber surface and the surrounding medium is enhanced. For photonic crystal fiber-optic sensors based on resonance of surface-isolated excitations, as the ambient refractive index increases, the effective refractive index of the isolated excitations on the surface of the gold film increases accordingly. According to the dispersion relation of light, the increase in the effective refractive index causes the resonance wavelength to shift towards the long wavelength direction, i.e., a red shift occurs. At the same time, due to the stronger interaction between the ambient refractive index and the optical field inside the fiber, more light energy is coupled into the surface equi-excitator modes, leading to an increase in the transmission loss of light in the fiber. This is due to the fact that under resonance conditions, the optical field energy is transferred from the conduction mode of the fiber to the surface equi-discrete exciton mode, which weakens the intensity of the light transmitted in the fiber and thus

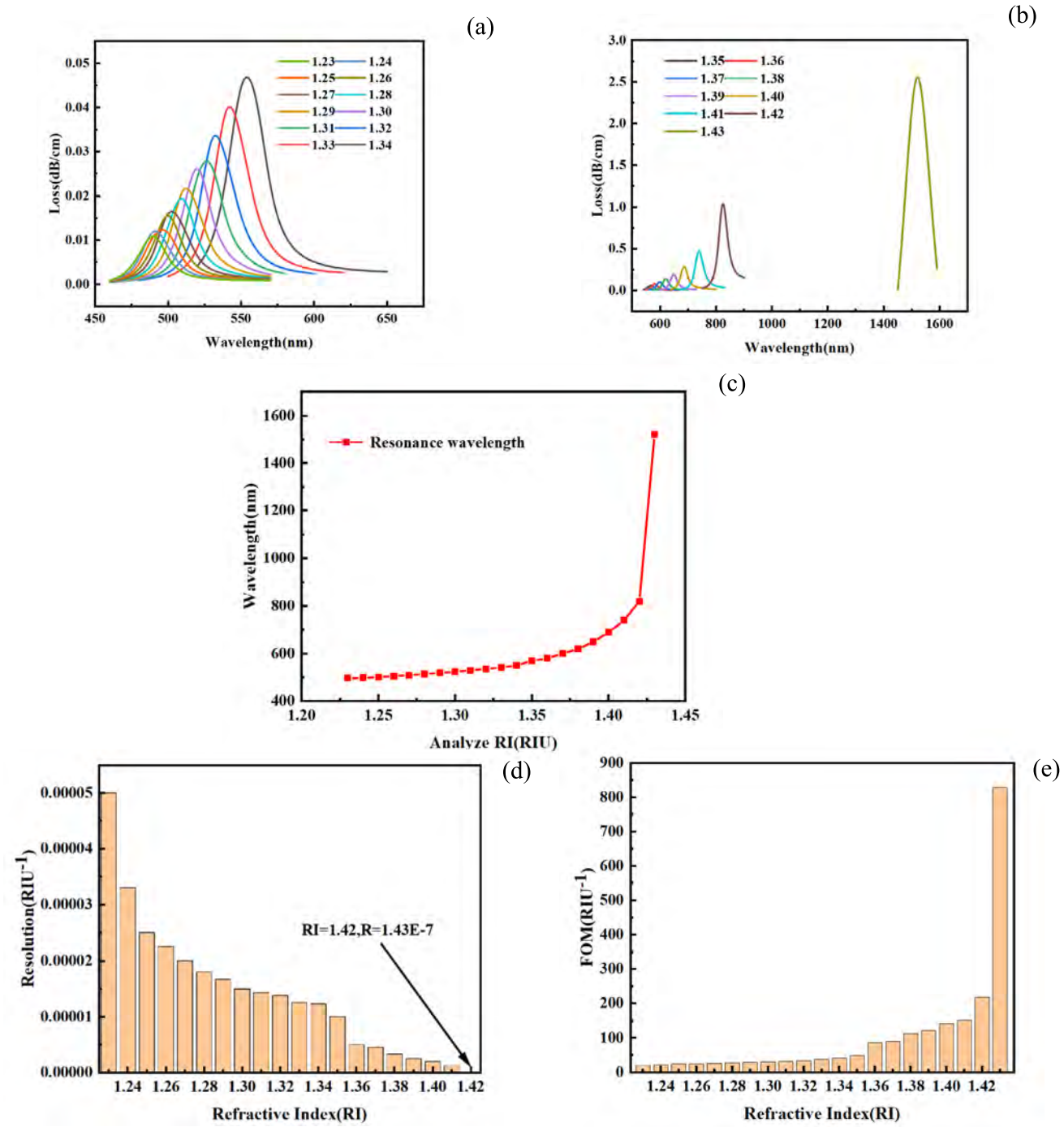

Fig. 7 **a** Loss spectra for *RI*s between 1.23 and 1.43; **b** loss spectra for *RI*s between 1.35 and 1.43; **c** variation of resonance wavelengths for refractive indexes of 1.23–1.43; **d** resolution of the PCF-SPR sensor; and **e** FOM for different analyte *RI*s

manifests itself as an increase in loss in the loss spectrum. In the refractive index range of 1.42 to 1.43, the coupling between the guided mode and the surface-isolated exciton mode of the fiber reaches a more optimal state, which makes the effective refractive indices of the two modes more matched, thus increasing the coupling efficiency between the modes. When the mode coupling is enhanced, a small change in the ambient refractive index causes a large shift in the resonance wavelength, which in turn improves the sensitivity of the sensor. The maximum loss of the sensor

Table 1 Table 1 Comparison of the sensing characteristics of different sensors

Refs.	Metals	Year	WS (nm/RIU)	Range of na	Structures
[32]	Au	2021	4200	1.32-1.41	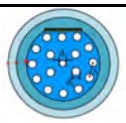
[33]	Au	2021	12719	1.43-1.49	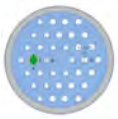
[34]	Au-TiO_2	2022	6000	1.33-1.39	
[35]	Au-TiO_2	2023	12500	1.37-1.41	
[36]	Au	2024	8000	1.33-1.39	
This work	Au	2024	70000	1.23-1.43	

is only 2.59 dB/cm, indicative of low energy loss during transmission as well as high transmission efficiency. Figure 7 (c) shows that the resonance wavelength increases with *RI* because the effective *RI* of the SPP mode rises, whereas the effective *RI* of the fiber-core mode remains largely unaltered. According to Eq. (4), the sensor exhibits a maximum sensitivity of 70,000 nm/*RIU* and an average sensitivity of 5150 nm/*RIU* in the *RI* range of 1.23–1.43. In addition, the resolution is significantly lower. According to Eq. (5), the resolution for $RI = 1.42$ is 1.43×10^{-7}, as shown in Fig. 7 (d). Moreover, Eq. (6) shows that the *FOM* is 834.4 RIU^{-1} at $RI = 1.43$ (Fig. 7(e)), confirming the excellent sensing characteristics.

Table 1 compares the properties of our sensor with those of similar PCF-SPR sensors in the recent. The superiority of our sensor is demonstrated.

Conclusion

A PCF-SPR sensor coated with a gold film with high sensitivity and low loss is designed and analyzed using the finite element method. In the analyte refractive index range between 1.23 and 1.43, the maximum and average wavelength sensitivities of the sensor are 70,000 nm/*RIU* and 5150 nm/*RIU*, respectively. Furthermore, it exhibits a resolution of 1.43×10^{-7} and an *FOM* of 834.4 RIU^{-1}. The performance of the *RI* sensor is superior to that of similar sensors in the literature, rendering it suitable for a variety of applications, including biosensing, virus detection, and organic chemistry.

Author Contribution Fengrui Yang : Conceptualization, Methodology, Software, Writing- Original Draft,Validation,Data Curation,Resources.

Jingwei Lv: Formal analysis.Wei Liu: Validation.Jianxin Wang: Methodology.Xili Lu: Validation.Lin Yang: Supervision. Qiang Liu: Software, Validation. Paul K. Chu: Resources, Project administration.Chao Liu: Funding acquisition,Conceptualization, Writing- Reviewing and Editing.

Funding This work was jointly supported by the Heilongjiang Provincial Natural Science Foundation of China [JQ2023 F001], National Natural Science Foundation of China [12304480], Local Universities Reformation and Development Personnel Training Supporting Project from Central Authorities, Natural Science Foundation of Heilongjiang Province [LH2021 F007], China Postdoctoral Science Foundation funded project [2020M670881], as well as City University of Hong Kong Donation Research Grants [DON-RMG 9229021 and 9220061].

Data Availability No datasets were generated or analysed during the current study.

Declarations

Competing interests The authors declare no competing interests.

References

1. Almewafy BH, Areed NFF, Hameed MFO et al (2019) Modified D-shaped SPR PCF polarization filter at telecommunication wavelengths. Optics and Quantum Electronics 51(1):193
2. Yasli A, Ademgil H, Haxha S, Aggoun A (2020) Multi-channel photonic crystal fiber based surface plasmon resonance sensor for multi-analyte sensing. IEEE Photonics J 12(1):1–15
3. Shakya AK, Ramola A, Singh S, Van V (2022) Design of an ultra-sensitive bimetallic anisotropic PCF SPR biosensor for liquid analytes sensing. Opt Express 30(6):9233–9255
4. Chaudhary VS, Kumar D, Kumar S (2021) Gold-immobilized photonic crystal fiber-based SPR biosensor for detection of malaria disease in human body. IEEE Sens J 21(16):17800–17807
5. Abdelghaffar M, Gamal Y, El-Khoribi RA et al (2023) Highly sensitive V-shaped SPR PCF biosensor for cancer detection. Optics and Quantum Electronics 55(1):472
6. Fei Y, Luo B, An M et al (2024) Highly sensitive surface plasmon resonance refractive index sensor based on D-shaped dual core photonic crystal fiber with ITO film. Plasmonics 19(6):1633–1647
7. Wang G, Lu Y, Duan L, Yao J (2021) A refractive index sensor based on PCF with ultra-wide detection range. IEEE J Sel Top Quantum Electron 27(4):1–8
8. Haihao FC, Liu C, Luhui X et al (2023) Surface plasmon resonance sensor composed of micro-nano optical fibers for high-sensitivity refractive index detection. J Opt Soc Am A 40(11):2177–2186
9. Zuhayer A, Elnaby A, Ahammad SH et al (2022) A gold-plated twin core D-formed photonic crystal fiber (PCF) for ultrahigh sensitive applications based on surface plasmon resonance (SPR) approach. Plasmonics 17(8):2089–2101
10. Doudou Wang Y, Zhang Y, Qi Y et al (2022) Tunable surface plasmon resonance sensor based on graphene-coated photonic crystal fiber in terahertz. Appl Opt 61(22):6664–6670
11. Wu H, Song Y, Sun M, Wang Q (2023) Simulation of high-performance surface plasmon resonance sensor based on D-shaped dual channel photonic crystal fiber for temperature sensing. Materials 16(1):37
12. Wang J, Pei L, Wu L et al (2020) A polarization-independent SPR sensor based on photonic crystal fiber for low RI detection. Plasmonics 15(2):327–333
13. Abrar Islam F, Haider F, Aoni RA et al (2021) U-grooved dual-channel plasmonic sensor for simultaneous multi-analyte detection. J Opti Soc Am B 38(11):3055–3063
14. El-Saeed AH, Khalil AE, Hameed MFO et al (2019) Highly sensitive SPR PCF biosensors based on Ag/TiN and Ag/ZrN configurations. Opt Quant Electron 51(1):56
15. Kumar S, Kumar D (2022) Sensitivity measurement based on the refractive index detection of dual-coated PCF SPR sensor. MAPAN - J Metrol Soc India 37(4):435–441
16. Gupta A, Singh T, Singh RK et al (2023) Numerical analysis of coronavirus detection using photonic crystal fibre-based SPR sensor. Plasmonics 18(2):577–585
17. Tiesheng Wu, Shao Y, Wang Y et al (2017) Surface plasmon resonance biosensor based on gold-coated side-polished hexagonal structure photonic crystal fiber. Opt Express 25(17):20313–20322
18. Xin Yan Y, Zhao Y, Cheng T, Rao Fu (2023) Surface plasmon resonance sensor for refractive index and temperature measurement based upon a double-sided polished microstructured fiber. Instrum Sci Technol 51(3):303–318
19. Hasan MS, Kalam MAE, Faisal M (2024) PCF based four-channel SPR biosensor with wide sensing range. IEEE Trans Nanobiosci 23(2):233–241
20. Han H, Hou D, Zhao L et al (2020) A large detection-range plasmonic sensor based on an H-shaped photonic crystal fiber. Sensors 20(4):1009
21. Zhang XL, Liu Y, Fan T et al (2017) Design and performance of a portable and multichannel SPR device. Sensors 17(6):1435
22. Majeed MF, Ahmad AK (2024) Design and analysis of a dual-core PCF biosensor based on SPR for cancerous cells detection. Optics and Quantum Electronics 56(1):1030
23. Manickam P, Senthil R (2022) Numerical investigation of side-polished SPR PCF sensor for urine analysis. Plasmonics 17(8):2023–2030
24. Mitu SA, Aktar MN, Ibrahim SM et al (2022) Surface plasmon resonance-based refractive index biosensor: an external sensing approach. Plasmonics 17(6):1581–1592
25. Khodatars Dashtmian MR, Fallahi V, Olyaee S et al (2024) Highly sensitive dual-side polished SPR PCF sensor for ultra-wide analyte range in the visible to near-IR operating band. Optics and Quantum Electronics 56(1):1187
26. Famei Wang M, Zou M, Liao C et al (2023) Three-dimensional printed microcantilever with mechanical metamaterial for fiber-optic microforce sensing. APL Photonics 8(9):096108
27. Famei Wang M, Zou M, Liao C et al (2024) Force sensing characteristic research based on fiber-optic end-face microcantilever probe. Photonic Sensors 14:240204
28. Jingwei Lv Y, Ren Y, Wang D et al (2024) Optical switching with high- Q Fano resonance of all-dielectric metasurface governed by bound states in the continuum. Opt Express 32(18):28334–28347
29. Jianxin Wang X, Lu X, Mi C et al (2024) Ultra-high sensitivity photonic crystal fiber sensor based on dispersion turning point sensitization of surface plasmonic polariton modes for low RI liquid detection. Opt Express 32(21):32895–32908
30. Jingwei Lv W, Li J, Wang J et al (2024) High-sensitivity strain sensor based on an asymmetric tapered air microbubble Fabry-Pérot interferometer with an ultrathin wall. Opt Express 32(11):19057–19068
31. Liu W, Liu C, Wang JX et al (2023) Surface plasmon resonance sensor composed of microstructured optical fibers for monitoring of external and internal environments in biological and environmental sensing. Results in Physics 47:106365
32. Yang H, Liu M, Chen Y et al (2021) Highly sensitive graphene-Au coated plasmon resonance PCF sensor. Sensors 21(3):818
33. Yan X, Wang Y, Cheng T, Li S (2021) Photonic crystal fiber SPR liquid sensor based on elliptical detective channel. Micromachines 12(4):408

34. Islam N, Masum MMU, Arif MFH et al (2022) Enhanced sensitivity of open channel SPR-based PCF sensor employing plasmonic materials for analyte sensing. Plasmonics 17(8):2075–2087
35. Tuaimah AM, Taher HJ, Tahhan SR et al (2023) Plasmonic D-shaped bimetallic coating refractive index sensor. Plasmonics 18(9):2393–2404
36. Walid A, Roy T, Hasan MM et al (2024) Design and performance analysis of a highly sensitive photonic crystal fiber based plasmonic sensor. Opt and Quant Electron 56(1):1042